Wind Effects on Shoaling Wave Shape

FALK FEDDERSEN

Scripps Institution of Oceanography, La Jolla, California

FABRICE VERON

Graduate College of Marine Studies, University of Delaware, Newark, Delaware

(Manuscript received 12 May 2004, in final form 16 November 2004)

ABSTRACT

Near the shore, cross-shore winds strongly affect the location of the break point and the breaking-wave height. From casual observation from the beach, wind direction (onshore or offshore) and speed also appear to affect wave shape (i.e., skewness and asymmetry), although as of yet this effect has not been quantified near the shore. The effect of wind on shoaling wave shape is investigated with laboratory experiments using monochromatic waves and onshore-directed wind. Wind increases the shoaling wave energy at discrete multiples of the primary frequency and has a significant effect on the wave shape at both a deeper and shallower shoaling locations. At the shallower location, the ratio of wave energy at 2 times the primary frequency to the primary frequency is also a function of wind speed, indicating interaction between the wind and the nonlinear wave shoaling process. Nearshore wave models do not account for these wind effects. Incorrect predictions of third-order velocity moments (wave shape), believed to control wave-driven sediment transport, would result in incorrect beach morphological evolution predictions.

1. Introduction

In the open ocean, it has long been recognized that surface waves are generated by the wind (e.g., Csanady 2001). Yet, wind-wave generation and attenuation are still an active area of research (e.g., Miles and Ierley 1998; Belcher 1999; Donelan 1999; Peirson et al. 2003) almost 50 years after the pioneering work of Miles (1957) and Phillips (1957). The interaction of the wind with the (long) swell waves also is of interest. Laboratory studies with small wave age c/u_* (c is the wave phase speed and u_* is the wind friction velocity) have shown that wind-wave generation is reduced in the presence of swell (e.g., Phillips and Banner 1974; Donelan 1987, 18–23). Several mechanisms have been proposed to explain this reduction in wind-wave growth, including enhanced breaking (Phillips and Banner 1974), resonant nonlinear interactions (Masson 1993), and swell–wind coupling (Chen and Belcher 2000). In contrast to the laboratory, where wind–swell coupling can be strong, the open-ocean wave age is typically large and the wind–swell coupling is presumed weak (Chen and Belcher 2000).

However, near the shore (within 0.5 km of the coast or at <10-m depth) the wave age is reduced as the phase speed of the shoaling waves decreases, and increased coupling between the waves and the wind is expected. In addition, the wind direction often is not aligned with the waves because of factors such as the sea breeze or mesoscale atmospheric phenomena, and wave nonlinearity increases during shoaling. The wind direction at the coast has a strong effect on the location of the break point and the breaking-wave height (and thus also on the distribution of the mean alongshore current). Douglass (1990) blew both onshore and offshore wind over a laboratory nearshore environment with a planar slope. The primary findings were that onshore (offshore) winds (a) moved the break-point location farther offshore (onshore) and (b) decreased (increased) the breaking-wave height-to-depth ratio γ_b. Changes in break-point location were as large as 40% and changes in γ_b were up to 100% for the range of wind speeds considered. This result implies that with

Corresponding author address: Falk Feddersen, Integrative Oceanography Division, Scripps Institution of Oceanography, University of California, San Diego, La Jolla, CA 92093-0209.
E-mail: falk@coast.ucsd.edu

offshore wind not only do waves break closer to shore, but they have larger breaking-wave heights. Similar laboratory results also were found by King and Baker (1996).

Regular beach users also know that the wind can have a strong effect on shoaling wave shape. A similar phenomenon was observed by Leykin et al. (1995) with wind-generated (nonshoaling) deep-water laboratory waves at a range of fetches and wind speeds ranging between 7 and 21 m s^{-1}. The wave skewness

$$S = \langle \zeta^3 \rangle / \sigma^3,$$

where ζ is the surface elevation, $\langle\ \rangle$ is an averaging operator, and σ^2 is the surface elevation variance, varied weakly and did not have a particular dependence on inverse wave age u_*/c. The wave asymmetry $A = \langle \zeta_H^3 \rangle / \sigma^3$, where ζ_H is the Hilbert transform of ζ, varied strongly and had a roughly linear relationship with the inverse wave age u_*/c. This change in asymmetry resulted chiefly from changes in the biphase at the peak frequency. If such an effect is observable for wind-generated deep-water waves, then it likely occurs in the more nonlinear and the reduced wave age of shallow-water shoaling waves. Except for the observations of Douglass (1990) and King and Baker (1996), to our knowledge, no controlled laboratory nearshore wave measurements have been made with varying wind direction and speed.

Here results from a limited pilot experiment intended to gauge the effect of wind on shoaling wave shape are reported. Although only onshore winds could be generated, wind had a substantial effect on shoaling wave shape, which appears to be stronger in shallower water. Potential implications for wave and sediment transport modeling are discussed.

2. Experiment description

A steep beach (slope 1:8) was installed at one end of the 37-m-long University of Delaware wind-wave tank. Monochromatic waves with period $f_p = 0.8$ Hz were generated and propagated in depth $h = 0.64$ m ($kh = 1.7$; k is the wavenumber) to the beach. Because the Ursell number [$\mathrm{Ur} = (H/h)/(kh)^2$] is small ($\mathrm{Ur} < 0.06$), wave-maker-generated free harmonics are likely negligible relative to forced harmonics in the shoaling regions sampled (Flick and Guza 1980). Winds up to 8 m s^{-1} in the direction of wave propagation were subsequently generated, and wind speed U was measured in the center of the tank 30 cm above the still-water level. Wind friction velocity u_* was not measured. At these wind speeds, which are much weaker than those used by Leykin et al. (1995), no whitecapping or microbreaking was observed. Water surface elevation ζ was measured by a capacitance wave gauge at two locations: location I with $h = 0.37$ m where the waves began shoaling ($kh = 1.2$ and $H/h \approx 0.28$) and location II with $h = 0.23$ m ($kh = 0.85$ and $H/h \approx 0.5$). Both locations I and II were seaward of the break point for all wind speeds. The surface elevation data are used to calculate energy spectra $E(f)$, bispectra $B(f_1, f_2)$ (e.g., Elgar and Guza 1985), wave height H [from an integral of $E(f)$], skewness S, and asymmetry A. Skewness and asymmetry are related to integrals of the real and imaginary parts of the bispectrum, respectively. The bispectrum is discussed through the bicoherence $b^2(f_1, f_2)$ and biphase $\beta(f_1, f_2)$, which, along with data analysis details, are reviewed in the appendix.

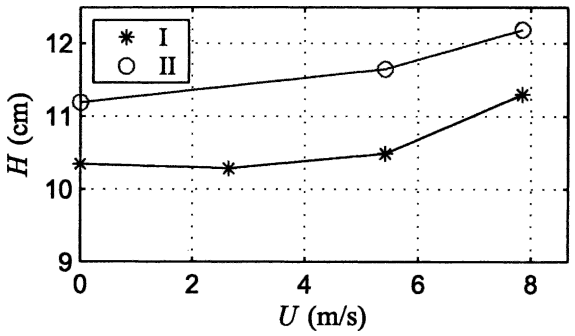

FIG. 1. Wave height H vs wind speed at location I (asterisks; deep shoaling $H/h \approx 0.28$) and location II (open circles; before the break point $H/h \approx 0.5$).

3. Results

At both locations I and II, wave height H increased modestly with wind speed (Fig. 1) as the wind inputs energy into the waves over the length of the tank. Even at the strongest wind speeds at the deeper location I, the spectrum $E(f)$ is made up of a strong peak at the primary frequency f_p and harmonics from $2f_p$ to $8f_p$ with little energy between peaks (Fig. 2). Almost all of the increased H with wind (Fig. 1) is a result of wind energy input to the wave field at discrete frequencies (nf_p, where $n = 1, 2, \ldots$) and not input broadly in frequency space (Table 1). This effect has been observed previously (e.g., Phillips and Banner 1974; Donelan 1987, 18–23). Small-scale wind-wave breaking (e.g., Phillips and Banner 1974) cannot explain this phenomenon because no breaking was visually observed in the wind-wave tank.

With no wind ($U/c = 0$), the asymmetry at location I is near zero but the skewness is nonzero (Figs. 3a,b) indicating that shoaling has just begun. At the shallower location II for $U/c = 0$, the skewness and asym-

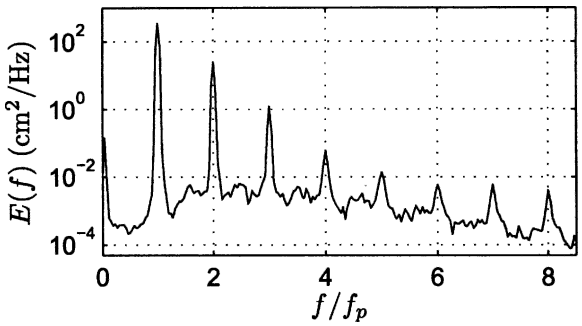

FIG. 2. Wave energy spectra vs normalized frequency f/f_p (f_p = 0.8 Hz) at location I during the strongest winds (U = 8 m s^{-1}).

TABLE 1. Changes in spectral energy levels $\Delta E(f)$ between U = 8 m s^{-1} and U = 0 m s^{-1} integrated over the spectral peaks $\int_p \Delta E(f)\, df$ and valleys $\int_v \Delta E(f)\, df$ (e.g., Fig. 2) at locations I and II. The integral over each spectral peak and valley has width $3df$ (df = 0.03 Hz) and $22df$, respectively. The integrals are performed over the first five peaks and valleys, respectively.

Location	$\int_p \Delta E(f)\, df$	$\int_v \Delta E(f)\, df$
I	2.59 cm^2	0.0084 cm^2
II	2.69 cm^2	0.0045 cm^2

metry have larger magnitudes as a result of shoaling nonlinear wave interactions (e.g., Elgar and Guza 1985). However, when wind is present, the shape of the wave is dramatically altered. At the deeper location I, the skewness slightly decreases with the ratio U/c (asterisks in Fig. 3a), but, similar to deep-water laboratory observations of wind waves (Leykin et al. 1995), the asymmetry is more strongly affected by the wind (asterisks in Fig. 3b), resulting in more pitched-forward waves. At the shallower location II, both the skewness and asymmetry of the shoaling waves are affected by the onshore wind (circles in Figs. 3a,b). The magnitude of asymmetry variation at both locations (about 0.2) is similar. The wind-induced change in wave shape also is evident in the mean wave profiles over a single period (Fig. 4). The wave shape changes are possibly simply due to the wind-induced increased incident H resulting in increased shoaling nonlinearity, and thus wave shape change. However, as discussed in section 4, this appears unlikely. This U/c range is applicable to a natural nearshore environment.

At both locations and for all wind speeds, the bicoherence $b^2(f_p, f_p)$ is high (≥ 0.98), implying very strong phase coupling between the primary frequency f_p and $2f_p$. The bicoherence is highly significant out to ($5f_p$, $5f_p$) for all cases, indicating that wind energy is not input into freely propagating waves. Increased wind does not decrease the $b^2(f_p, f_p)$; thus all energy input by the wind into the wave field (at $2f_p$) is also phase

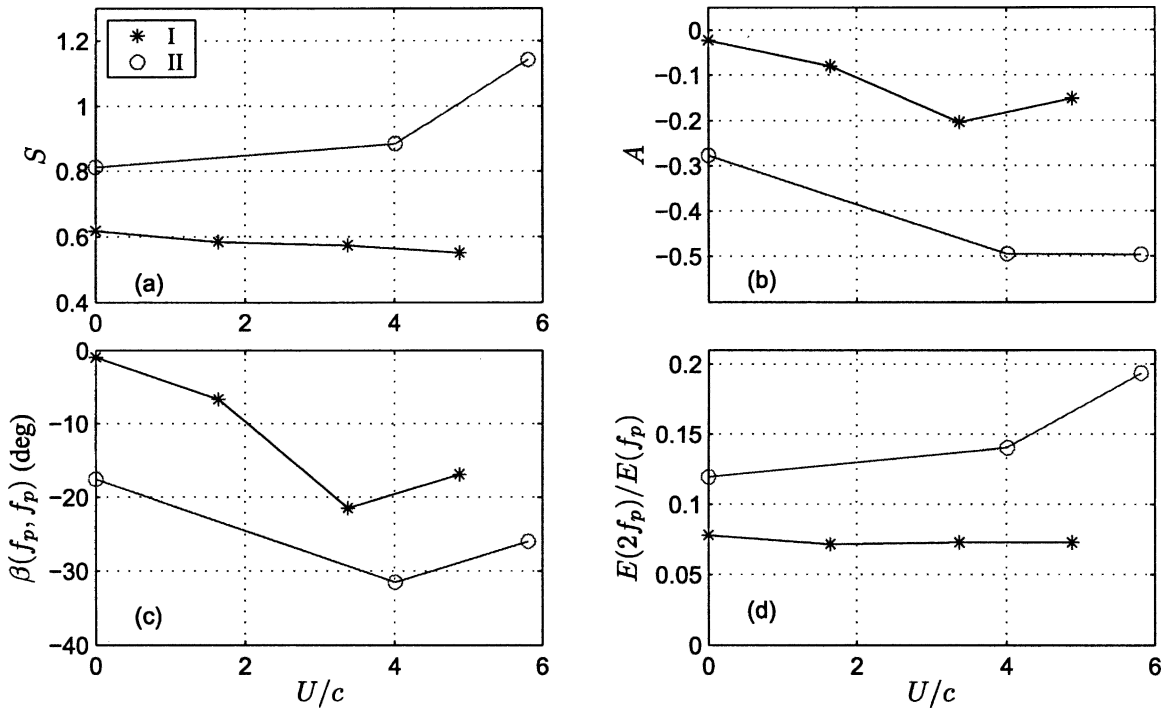

FIG. 3. (a) Skewness S, (b) asymmetry A, (c) biphase $\beta(f_p\ f_p)$ (°), and (d) $E(2f_p)/E(f_p)$ ratio vs the ratio of wind speed U to wave phase speed c (U/c) at locations I and II.

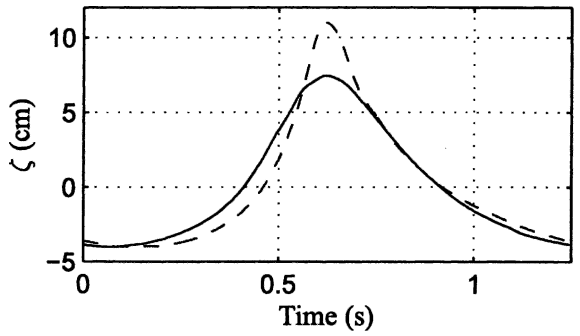

FIG. 4. Mean wave profile (averaged over 260 waves) vs time at location II; with $U/c = 0$ (solid) and $U/c \approx 6$ (dashed). The wave period is T = 1.25 s.

coupled to the primary frequency. With no wind ($U/c = 0$), the biphase $\beta(f_p, f_p)$ evolves from near 0° at location I to −18° at location II, consistent with wave-shoaling biphase evolution toward −90° (Elgar and Guza 1985, 1986). The biphase $\beta(f_p, f_p)$ is affected strongly by the wind (Fig. 3c). At location I and II, $\beta(f_p, f_p)$ varies by 20° and 14°, respectively, is highly significant (appendix), and results in more asymmetric waves. This $\beta(f_p, f_p)$ variation is about 40% of and has the sense (with U/c) of biphase variation as observed by Leykin et al. (1995) for wind-generated deep-water waves under much stronger winds. The decrease in $|\beta|$ for $U/c > 4$ is not understood but is statistically significant.

At location I, the ratio of wave energy at $2f_p$ to f_p, $E(2f_p)/E(f_p)$, is relatively constant with U/c (asterisks in Fig. 3d), although $E(f_p)$ and $E(2f_p)$ vary by 20% with U/c. The constant $E(2f_p)/E(f_p)$, together with the $\beta(f_p, f_p)$ variation, explains the small decrease with U/c in observed skewness (asterisks in Fig. 3a) as the asymmetry (asterisks in Fig. 3b) increases, because skewness and asymmetry are related to integrals of the real and imaginary parts of the bispectrum, respectively. The constant $E(2f_p)/E(f_p)$ could result from wind inputing energy at the primary frequency f_p, which then generates the bound harmonic. However, this does not explain the location-I biphase change (Fig. 3c). As an alternative, wind could be contributing energy to both frequencies proportionally. However, at location II, the ratio $E(2f_p)/E(f_p)$ increases (by 62%) with U/c (circles in Fig. 3d), and a similar increase with wind is also observed with the ratio $E(3f_p)/E(f_p)$ (by 140%; not shown). This is not due to wind generation along the tank, because at the deeper location I the ratio is constant. Instead, something fundamental about the wave-shoaling process (reduced wave age and the increased nonlinearity) allows wind energy to be preferentially put into phase-coupled harmonics of the wave. For a phase-coupled process, this change in $E(2f_p)/E(f_p)$ also affects the skewness and asymmetry (even with no biphase variation).

4. Discussion

As mentioned in section 3, an alternative explanation for the changes in wave shape is that the wind-induced increased (by 10%) incident wave height H increases the shoaling nonlinearity, resulting in the observed wave shape changes. However, this alternative explanation appears unlikely for a number of reasons. First, recall the wind affects wave shape for deep-water wind-generated waves (Leykin et al. 1995). Also, if the wind only increased the incident H, then the ratio of breaking-wave height to depth (γ_b) is expected to remain approximately constant. However, γ_b changes dramatically (up to 100%) with offshore to onshore wind (Douglass 1990), demonstrating that, for the same H, the wind affects wave breaking and by implication the shoaling wave shape. Furthermore, if this alternative explanation were valid for the conditions in section 3, then at location I, along with the observed changes in biphase (Fig. 3c), because of increased nonlinearity, a corresponding change in $E(2f_p)/E(f_p)$ is expected. At location I, this is not observed (asterisks in Fig. 3d). Last, an extra run with no wind ($U/c = 0$) but with increased incident wave height resulted in $H = 11.4$ cm at location II, halfway between the $U/c = 0$ and $U/c = 4$ location-II wave heights (circles in Fig. 1). However, with no wind ($U/c = 0$) the change in biphase $\beta(f_p, f_p)$ is $< 1.5°$ (not statistically significant) with the two different incident wave heights. In contrast, with onshore wind ($U/c = 4$), there is a (highly significant) $>15°$ change in $\beta(f_p, f_p)$. These reasons together strongly suggest that the observed changes in wave shape are the result of wind interacting with the shoaling waves and are not due to the alternative explanation.

The limited experiment data prevent conclusions from being quantified further. The wind-wave tank could not be configured for offshore-directed wind. The steep beach (1:8) configuration is not ideal, because in the shoaling region the slowly varying approximation is not valid. In addition, such steep beaches are not realistic. However, with a smaller beach slope, the wind effects on wave shape are arguably larger because the wind and waves would have a greater propagation distance over which to interact. These issues require further investigation.

Nearshore wave models do not yet take these wind effects into account. Without them, wave-model predictions of break-point location, wave height (Douglass 1990), and third-order wave moment (skewness and asymmetry) can be degraded significantly. Sediment

transport models often are based on third-order moments (e.g., Gallagher et al. 1998). For example, Elgar et al. (2001) demonstrated that onshore sandbar migration could be related to the wave asymmetry, and Hoefel and Elgar (2003) showed that adding a wave-asymmetry-related (acceleration skewness) term (Drake and Calantoni 2001) resulted in improved modeling of onshore bar migration. Therefore wind, through its effect on wave shape, also could affect sediment transport. By ignoring wind effects, sediment transport models may predict incorrect beach morphological evolution. Different beaches around the world experience different types of wind conditions (e.g., onshore–offshore diurnal sea breeze or regular trade winds). Thus the local wind climate possibly could be a determining factor for the beach morphological conditions (i.e., whether the beach is barred).

The mechanism for wind to affect shoaling waves is presumably through the dynamic surface boundary condition for irrotational gravity waves. It has long been recognized that wind-induced varying pressure boundary conditions along the wave crest and trough can theoretically lead to wave growth (e.g., Miles 1957; Phillips 1957), though the details of how a turbulent airflow accomplishes this still are not well understood. With nonlinear shoaling waves, the wind-induced surface pressure may change the phase relationship and energy ratio (e.g., Figs. 3c,d) of the second (and higher) harmonics to the peak wave frequency. Modified wave-generation theories that include wind effects at higher order (i.e., harmonics of the primary wave) may be able to explain the observed change in wave shape with the wind.

5. Summary

Onshore-directed wind up to 8 m s^{-1} was blown over monochromatic shoaling laboratory waves. No whitecapping or microbreaking was observed. Wave shoaling reduces the wave age, suggesting increased coupling between wind and the waves, and increases the wave nonlinearity. Wind increased the shoaling wave height (by 10%) by putting energy into discrete multiples of the peak frequency. Wind also affected the shoaling wave shape. At the deeper location, only the asymmetry was affected; at the shallower location near the break point, both the skewness and asymmetry were changed. At both locations, this change in wave shape was reflected in significant biphase variations. At the shallower location, the wind preferentially puts energy into phase-coupled harmonics, which also changes wave shape. This preferential energy input was not observed at the deeper location, indicating that it is a result of the nonlinear shoaling process interacting with the wind.

Although this experimental dataset is limited, the results are robust and are of interest to the nearshore wave and sediment transport modeling communities. Future laboratory experiments that include offshore wind and cover a greater parameter range are desirable to quantify wind effects on wave shape further.

Acknowledgments. This work was supported by a UCSD Academic Senate Award, NOPP, NSF, and ONR; J. T. Kirby, R. T. Guza, Steve Elgar, Steve Henderson, R. E. Flick, and anonymous reviewers provided valuable feedback.

APPENDIX

Spectra and Bispectra Definitions and Data Processing

Writing the Fourier coefficients as $A(f)$, the spectrum (appropriately normalized) is defined as $E(f) = \langle |A(f)|^2 \rangle$, where $\langle\ \rangle$ is an averaging operator. The bispectrum is defined as (Kim and Powers 1979)

$$B(f_1, f_2) = \langle A(f_1)A(f_2)A^*(f_1 + f_2) \rangle,$$

where the asterisk denotes the complex conjugate. The bicoherence and biphase are given respectively by (Kim and Powers 1979)

$$b^2(f_1, f_2) = \frac{|B(f_1, f_2)|^2}{\langle |A(f_1)A(f_2)|^2 \rangle \langle |A(f_1 + f_2)|^2 \rangle} \quad \text{and}$$

$$\beta(f_1, f_2) = \arctan\left\{\frac{\text{Im}[B(f_1, f_2)]}{\text{Re}[B(f_1, f_2)]}\right\}.$$

The bicoherence varies between 0 and 1 and, for a three-wave system, represents the fraction of energy at $f_1 + f_2$ resulting from quadratic coupling from frequencies f_1 and f_2. Writing Fourier coefficients as $A(f) = |A(f)| \exp[i\theta(f)]$, the biphase $\beta(f_p, f_p)$ at the primary frequency is $2\theta(f_p) - \theta(2f_p)$ (Elgar and Guza 1985) and reveals whether the phase coupling leads to skewed ($\beta = 0°$) or more asymmetric ($|\beta| = 90°$) waves.

After wave-tank spinup, the wave gauges were sampled at 200 Hz for 325 s, and data were low-pass filtered with cutoff frequency of 20 Hz before calculating wave statistics. Spectral analysis was performed on data segments 32.5 s long, with 50% overlap, resulting in 38 degrees of freedom (dof). Based on the dof and the observed bicoherence, the true bicoherence and biphase at (f_p, f_p) are expected (with 95% confidence) to be within 0.02 and 3°, respectively, of the true $b^2(f_p, f_p)$ and $\beta(f_p, f_p)$ (Kim and Powers 1979; Elgar and Sebert

1989). Spectra were integrated over 2 times the frequency resolution ($df = 0.03$ Hz) to calculate the $E(f_p)/E(2f_p)$ ratios.

REFERENCES

Belcher, S. E., 1999: Wave growth by non-separated sheltering. *Eur. J. Mech. B/Fluids,* **18,** 447–462.

Chen, G., and S. E. Belcher, 2000: Effects of long waves on wind-generated waves. *J. Phys. Oceanogr.,* **30,** 2246–2256.

Csanady, G. T., 2001: *Air–Sea Interaction: Laws and Mechanisms.* Cambridge University Press, 239 pp.

Donelan, M. A., 1987: The effect of swell on the growth of wind waves. Johns Hopkins APL Tech. Doc. 8.

——, 1999: Wind-induced growth and attenuation of laboratory waves. *Wind-over-Wave Couplings, Perspectives and Prospects,* S. G. Sajjadi, N. H. Thomas, and J. C. R. Hunt, Eds., Clarendon Press, 356 pp.

Douglass, S. L., 1990: Influence of wind on breaking waves. *J. Waterw. Port Coastal Ocean Eng.,* **116,** 651–663.

Drake, T. G., and J. Calantoni, 2001: Discrete particle model for sheet flow sediment transport in the nearshore. *J. Geophys. Res.,* **106,** 19 859–19 868.

Elgar, S., and R. T. Guza, 1985: Observations of bispectra of shoaling surface gravity waves. *J. Fluid Mech.,* **161,** 425–448.

——, and ——, 1986: Nonlinear model predictions of bispectra of shoaling surface gravity waves. *J. Fluid Mech.,* **167,** 1–18.

——, and G. Sebert, 1989: Statistics of bicoherence and biphase. *J. Geophys. Res.,* **94,** 10 993–10 998.

——, E. L. Gallagher, and R. T. Guza, 2001: Nearshore sandbar migration. *J. Geophys. Res.,* **106,** 11 623–11 627.

Flick, R. E., and R. T. Guza, 1980: Paddle generated waves in a laboratory channel. *J. Waterw. Port Coastal Ocean Eng.,* **106,** 79–97.

Gallagher, E. L., S. Elgar, and R. T. Guza, 1998: Observations of sand bar evolution on a natural beach. *J. Geophys. Res.,* **103,** 3203–3215.

Hoefel, F., and S. Elgar, 2003: Wave-induced sediment transport and sandbar migration. *Science,* **299,** 1885–1887.

Kim, Y. C., and E. J. Powers, 1979: Digital bispectral analysis and its application to nonlinear wave interactions. *IEEE Trans. Plasma Sci.,* **1,** 120–131.

King, D. M., and C. J. Baker, 1996: Changes to wave parameters in the surfzone due to wind effects. *J. Hydraul. Res.,* **34,** 55–76.

Leykin, I. A., M. A. Donelan, R. H. Mellen, and D. J. McLaughlin, 1995: Asymmetry of wind waves studied in a laboratory tank. *Nonlinear Proc. Geophys.,* **2,** 280–289.

Masson, D., 1993: On the nonlinear coupling between swell and wind-waves. *J. Phys. Oceanogr.,* **23,** 1249–1258.

Miles, J. W., 1957: On the generation of surface waves by shear flows. *J. Fluid Mech.,* **3,** 185–204.

——, and G. Ierley, 1998: Surface-wave generation by gusty wind. *J. Fluid Mech.,* **357,** 21–28.

Peirson, W. L., A. W. Garcia, and S. E. Pells, 2003: Water wave attenuation due to opposing wind. *J. Fluid Mech.,* **487,** 345–365.

Phillips, O. M., 1957: On the generation of waves by turbulent wind. *J. Fluid Mech.,* **2,** 417–445.

——, and M. L. Banner, 1974: Wave breaking in the presence of wind drift and swell. *J. Fluid Mech.,* **66,** 625–640.